Journal of Molecular Structure 1227 (2021) 129576

Contents lists available at ScienceDirect

Journal of Molecular Structure

journal homepage: www.elsevier.com/locate/molstr

# Experimental and computational studies of di-$\mu$-chlorido-bis[chlorido(1,10-phenanthroline-K$^2$*N*,*N*′)nickel(II)] $NiCl_2(H_2O)(C_{12}N_2H_8)$: Crystal structure, quantitative analysis of the intermolecular interactions and electronic properties

Brahim El Bali[a], Mohammed Lachkar[b], Amani Direm[c,*], Esra Çetiner[d], Koray Sayin[d], Michal Dusek[e]

[a] *Independent scientist*
[b] *Laboratoire d'Ingénierie des Matériaux Organométalliques et Moléculaires, Unité Associée au CNRST (URAC 19), Faculté des Sciences, Université Sidi Mohamed Ben Abdellah, B.P.1796 (Atlas), 30000 Fès, Morocco*
[c] *Laboratory of Structure, Properties and Intermolecular Interactions LASPI2A, Department of Matter Sciences, Faculty of Sciences and Technology, Abbes Laghrour University Khenchela, 40.000 Algeria*
[d] *Department of Chemistry, Faculty of Science, Cumhuriyet University, 58140 Sivas, Turkey*
[e] *Institute of Physics of the Czech Academy of Sciences, Na Slovance 2, 182 21, Praha 8, Czech Republic*

ARTICLE INFO

*Article history:*
Received 2 September 2020
Revised 31 October 2020
Accepted 2 November 2020
Available online 3 November 2020

*Keywords:*
Ni(II) complex
Crystal structure
*Hirshfeld* surface analysis
MEP map
Quantum chemical calculations

ABSTRACT

$NiCl_2(H_2O)(C_{12}N_2H_8)$ was synthesized in solution and its structure was studied by single-crystal X-ray diffraction. It crystallizes in the monoclinic system (S. G.: $P2_1/n$), $Z = 4$, with the cell parameters (Å, °): $a = 12.6640(5)$, $b = 6.8322(3)$, $c = 14.2054(5)$ and $\beta = 93.569(3)$. The final residual factors of the refined structure model R/R$\omega$ were 0.031/0.082 for 2156 independent reflexions and 172 parameters. The crystal structure is described in terms of $Ni_2Cl_4(H_2O)_2(Phen)_2$ dimmers interacting through weak intermolecular O–H…Cl Hydrogen bonds. The 2D fingerprint plots, built using the *Hirshfeld* surface analysis, helped analyzing and quantifying all the intermolecular contacts and revealed the main intermolecular interactions around the title complex. The computational investigation was undertaken at M06–2X/6–31G(d)(LANL2DZ) level by using Gaussian.



## 1. Introduction

The molecule 1,10-phenantroline (**Phen**) and its different derivatives are considered as interesting ligands used in various chemical industries [1]. Heteroatomic group of Phen provides a binding site for different metal ions. It has a rigid structure and has two aromatic nitrogen atoms which contain unshared electronic pairs that can bind metals [2,3]. Due to its electron deficiency, Phen turns to be a good acceptor leading then to various applications such as catalysis, redox, photo-redox and biological activities [3–8]. Especially in supramolecular chemistry, Phen derivatives are reported to play a key role [9–11].

Metal complexes with 5-amino-1,10-phenantroline (**aphen**) were reported to be interesting potentiometric sensors, $M^{+2} = 3d$ transition metal, including Zn [12]. Moreover, Tammiku et al. reported that the complexation of magnesium halide $MgX_2$ with Phen is the reason for the disappearance of the red color of the complex RMgX(phen) near the titration end point [13]. The anticancer properties of the lanthanum compound [tris(1,10-phenanthroline) lanthanum(III)] trithiocyanate have been published by Heffeter et al. [14]. Recently, photochemical properties of a series of 1,10-phenantroline complexes have been reported [15]. Since phen is considered as a classic ligand used in coordination chemistry, which couples versatility in metal ion binding with atypical properties of its complexes, Phen-based metal complexes can interact with DNA in an intercalative fashion inducing, in some cases, DNA cleavage [16]. However, even with this last ability, molecular phen could not be medically used, due to its toxicity caused by inhibiting metalloenzymes via its chelating nitrogen atoms. Nonetheless, the toxicity has been bypassed for its attractive features coordinating with transition metals [17]. Alrejaa and Kaur published a review of the developments of phen ligands behaving as chemosensors for anions and cations. Their investigations yielded a database of various phen-derived receptors serving as chemosensors for various analytes

* Corresponding author.
*E-mail addresses:* amani_direm@yahoo.fr, d_amani_83@yahoo.fr (A. Direm).

https://doi.org/10.1016/j.molstruc.2020.129576
0022-2860/

in different solvents, with a correlation of results with photophysical properties for applications in the biological and environmental fields [18]. Recently, *Eni* et al. reported on the reaction of phen and dicyanamide ligands with $Co^{+2}$ and $Cu^{+2}$ nitrates resulting in the two complexes $[Co(phen)_2(NO_3)](dcg)\cdot(H_2O)$ and $[Cu(phen)(BMCA)](NO_3)$, with BMCA and dcg refer respectively to bis(methoxycarbimido)aminato and dicyanoguanidinate anions. The thermal and antimicrobial properties of these complexes have also been evaluated and DFT calculations were performed for better insights into the molecular interactions in the structures of these complexes with possible prediction of their electronic properties [19].

The present study is devoted to the investigation of a newly synthesized Ni(II)complex: $NiCl_2(H_2O)(Phen)$. The manuscript will provide its detailed crystal structure description, with the data correlated to the calculated ones and the *Hirshfeld* surface analysis of its intermolecular interactions. The studied complex was optimized at M06–2X/6–31G(d)(LANL2DZ) level. The structural parameters, molecular orbital energy diagram (MOED), contour plots of selected molecular orbitals, molecular electrostatic potential (MEP) map were examined in detail.

## 2. Materials and methods

### 2.1. Synthesis and crystallization

The crystals of the compound under investigation were obtained from an experiment aiming the preparation of a hybrid-phosphate based on phenanthroline. Concretely, 1 mL (20 mmol) of 1,10-Phenanthroline hydrochloride monohydrate $C_{12}H_8N_2\cdot HCl\cdot H_2O$ [Aldrich-Sigma, purity ≥ 99.5% (titration)] was added dropwise to a mixture made of $NiCl_2\cdot 6H_2O$ (10 mL, 100 mmol) and $H_3PO_3$ (10 mL, 100 mmol) both high quality reactants (Aldrich-Sigma, purity ≥ 99.5%) dissolved in distilled water. The slow evaporation at room temperature of the obtained solution gave rise to large green block-like crystals suitable for single-crystal X-ray diffraction.

### 2.2. Single crystal X-ray diffraction

The X-ray diffraction data for the title compound were collected at 298 K on a Rigaku Oxford Diffraction diffractometer, using a graphite monochromatized MoK$\alpha$ radiation ($\lambda$ = 0.71073 Å) collimated with Mo-Enhance collimator, and the Atlas S1 CCD detector. A numerical absorption correction based on the crystal shape was carried out with the program CrysAlis RED [20]. The structure was solved by the Direct Methods procedure of SIR97 [21] and refined by a full-matrix least-squares technique based on $F^2$ with Jana2006 [22]. Table 1 summarizes the crystallographic data and the experimental details about the data collection and the structure refinement. The structural graphics were sketched using DIAMOND program [23].

**Table 1**
Crystallographic data and details of X-ray diffraction analysis for $NiCl_2(H_2O)(C_{12}N_2H_8)$.

| | |
|---|---|
| $NiCl_2(H_2O)(C_{12}N_2H_8)$ | $Z = 4$ |
| $M_r$ (g/mol)= 325.8 | $F(000) = 664$ |
| Monoclinic, $P2_1/n$ | |
| Mo $K\alpha$ radiation, $\lambda$ = 0.71073 Å | $\theta$ = 4.5–66.9° |
| $a$ = 12.6640 (5) Å | $\mu$ = 6.19 mm$^{-1}$ |
| $b$ = 6.8322 (3) Å | $T$ = 120 K |
| $c$ = 14.2054 (5) Å | $\beta$ = 93.569 (9)° |
| $V$ = 1226.71 (8) Å$^3$ | 0.14 × 0.45 × 0. 54 mm$^3$ |
| 2156 reflections with $I > 2\sigma(I)$ | $h = -15\rightarrow15$ |
| $l = -16\rightarrow15$ | $k = -8\rightarrow7$ |
| Refinement on $F^2$ | Least-squares matrix: full |
| $R[F^2 > 2\sigma(F^2)]$ = 0.031 | w$R(F^2)$ = 0.082 |

Supplementary tables of the crystal structure and refinement, notably the full list of bond lengths and angles, and anisotropic thermal parameters have been deposited to the Cambridge Database, these data can be obtained free of charge using the link: www.ccdc.cam.ac.uk or from the CCDC, 12 Union Road Cambridge CB2 1EZ, UK; fax: +44 1223 336033; E-mail: deposit@ccdc.cam.ac.uk]. CCDC deposition number is **886031**.

### 2.3. Hirshfeld *surface calculation*

The *Hirshfeld* surfaces [24] around the title complex and their associated fingerprint plots were calculated using CrystalExplorer software [25].

### 2.4. Computational details

Computational calculations were performed by Gaussian and VEDA 4XX programs [26–29]. The title complex was optimized by using Gaussian programs. For this purpose, M06–2X method, one of the DFT hybrid functions, was used with mix basis set; LANL2DZ was used for the nickel atom and 6–31G(d) was used for the remaining atoms in the complex. The calculated IR spectrum was examined by using VEDA 4XX program.

## 3. Results and discussion

### 3.1. Crystal structure

The crystal structure reveals the presence of Ni-dimers with unusual coordination environments. The heteroleptic quasi-octahedral Ni-coordination consists of $NiN_2OCl_3$, where the two N sit in a *cis*-conformation relative to the main plane of the dimer and belong to $C_{12}N_2H_8$. The three Cl atoms occupy one side of the quasi octahedron, resembling to a *fac*-coordination. The oxygen atom from the water molecule is completing the six-fold coordination. The two quasi-octahedra, constructing the dimer, share a common edge of two Cl atoms. It is worth to be noted that a center of inversion is found between the Ni atoms and agrees with the distribution of coordinating atoms. The nominal composition suggests that Ni centers are charged +2, which corresponds to a $d^8$ electronic configuration. As the Ni–Ni distance is about 3.4 Å, a direct magnetic exchange is unlikely, but the most obvious is that the Ni–Cl–Ni super-exchange path is close to an ideal overlap of orbitals (90.062(1)°). Fig. 1 depicts the asymmetric unit

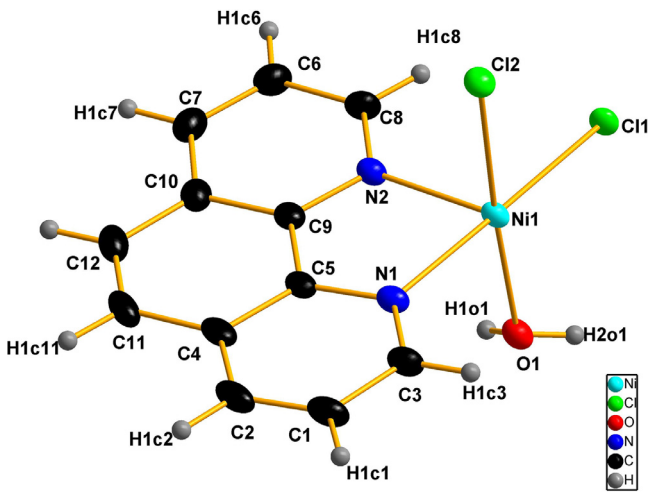


**Fig. 1.** Asymmetric unit in $NiCl_2(H_2O)(C_{12}N_2H_8)$.

in the complex $NiCl_2(H_2O)(Phen)$. The framework exhibits a distorted square-bipyramidal geometry where the metal $Ni^{+2}$ is coordinated through two apical chloride (Cl1) and two two imine nitrogen atoms (N1 and N2), and equatorial Cl2 and aqua O1 atom. Such octahedron share the edge Cl1-Cl1 to define dimmers "$Ni_2Cl_4(H_2O)_2(Phen)_2$".

The cohesion within the crystal packing of the title complex is governed by an intermolecular hydrogen bonding network (Table 2) within the cavity containing Ni and Cl, which results in long Ni–Cl distances ranging from 2.398 to 2.439 Å. The average distances Ni–Cl (2.4164 Å) and Ni–O (2.1247 Å) are comparable to such distances of the known compounds reported in the literature,

**Table 2**
Hydrogen-bond geometry (Å, °) in the title complex.

| *D—H···A* | *D—H* | *H···A* | *D···A* | *D—H···A* |
|---|---|---|---|---|
| *O1—H1o1···Cl2$^{i}$* | *0.78 (3)* | 2.41 (3) | 3.1821 (17) | 168 (3) |

*Symmetry code: (i) x, y − 1, z.*

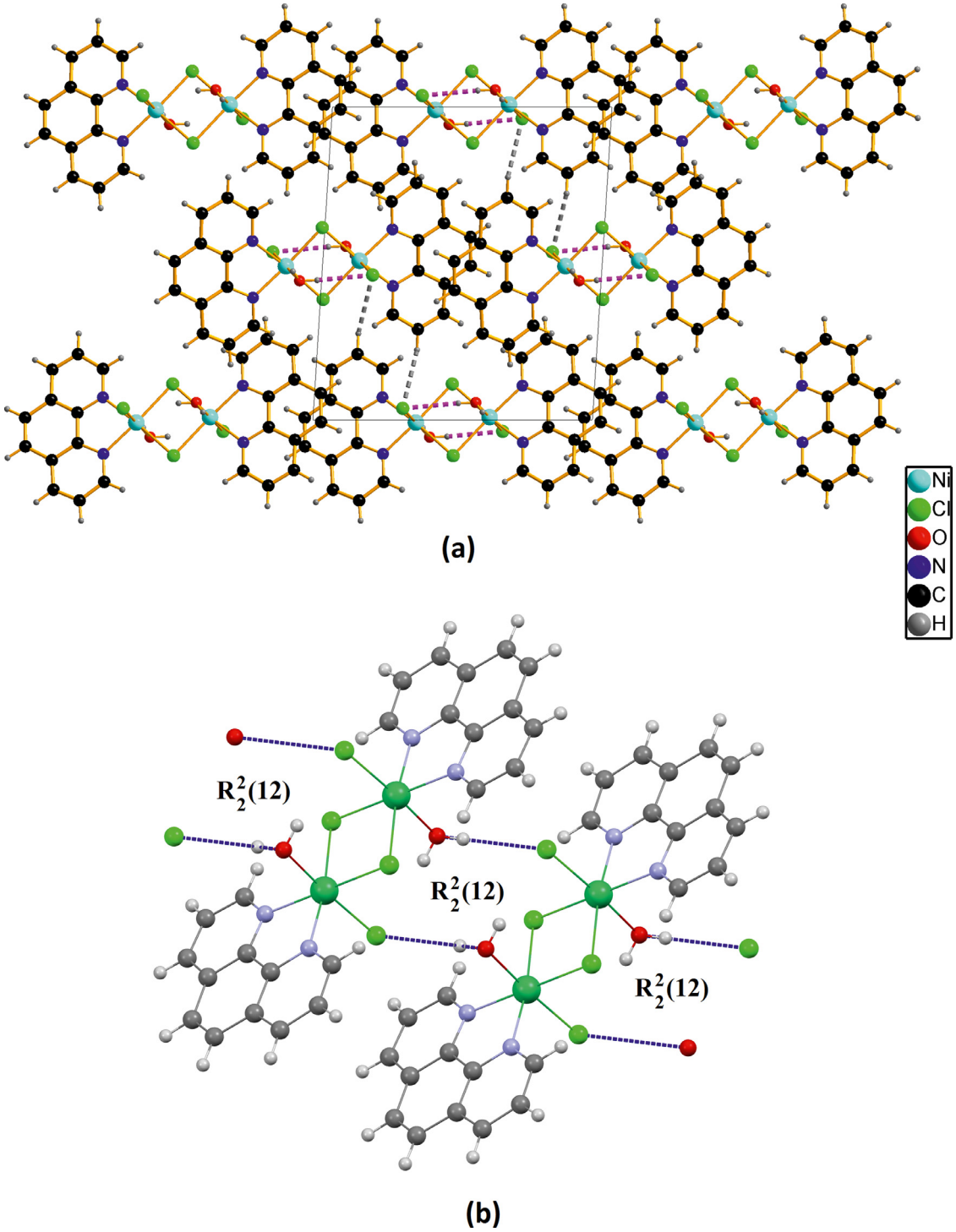


**Fig. 2.** (a) A view of the crystal structure onto the (*ac*) crystallographic plane; (b) Edge-fused centrosymmetric $R^2_2(12)$ first-level rings with the N–H…Cl hydrogen bonds shown as dashed lines.

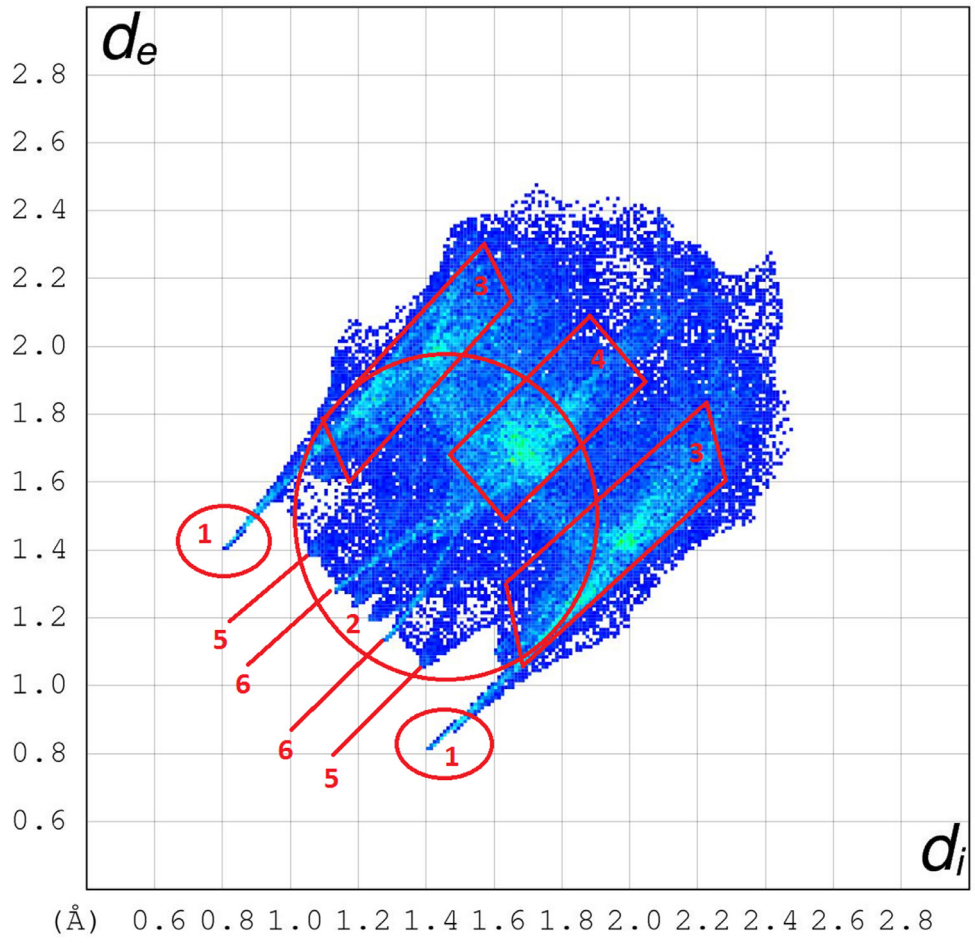


**Fig. 3.** 2D Fingerprint plots of the intermolecular interactions within the title compound's asymmetric unit. The decomposed plots were labelled.

specifically ⟨Ni–Cl⟩ are 2.426 Å in $NiCl_2$ [30], 2.398 Å in $NiCl_2{\cdot}2H_2O$ [31], 2.388 Å $NiCl_2{\cdot}4H_2O$ [32] and 2.360 Å in $NiCl_2{\cdot}6H_2O$ [33], while ⟨Ni-O⟩ are respectively 2.10 Å, 2.089 Å, 2.086 Å and 2. 048 Å in NiO [34], $NiCl_2{\cdot}2H_2O$ [31], $NiCl_2{\cdot}4H_2O$ [32] and $NiCl_2{\cdot}6H_2O$ [33].

Viewed thus along the direction [010], the crystal structure of $NiCl_2(H_2O)$(Phen) can be described in terms of the above defined dimmers "$Ni_2Cl_4(H_2O)_2(Phen)_2$" interconnected through weak intermolecular O–H…Cl hydrogen-bonds [O1-H1o1…Cl2: 2.41(3) Å], drawn as dashed lines in Fig. 2a. Each two complex molecules link together *via* two of the above mentioned hydrogen bond to generate alternating centrosymmetric edge-fused $R^2_2(12)$ first-level graph-set motifs (Fig. 2b), which alternate repeatedly through the [010] direction to form sheets consisting of parallel C(4) infinite chains [35].

### 3.2. Hirshfeld *surface analysis*

For each point on the *Hirshfeld* isosurface, two distances $d_e$ (the distance from the point to the nearest nucleus external to the surface) and $d_i$ (the distance to the nearest nucleus internal to the surface) are defined. Therefore, a normalized contact distance $d_{norm}$ [36,37] can be derived from the two distances ($d_e$ and $d_i$) and is given with respect to the following equation:

$$d_{norm} = \frac{d_i - r_i^{vdW}}{r_i^{vdW}} + \frac{d_e - r_e^{vdW}}{r_e^{vdW}}$$

Where, $r_i^{vdW}$ and $r_e^{vdW}$ are the *van der Waals* radii of the appropriate atoms which are internal and external to the *Hirshfeld* surface, respectively. The value of $d_{norm}$ is negative or positive when the intermolecular contacts are shorter or longer than the *van der Waals* radii, respectively. When $d_{norm}$ is mapped on the *Hirshfeld* surface, close intermolecular distances are characterized by three identically colored regions. Red regions stand for closer contacts and negative $d_{norm}$ value, blue regions represent longer contacts and positive $d_{norm}$ value, whereas white regions correspond to the contacts distance, which is exactly equal to the *van der Waals* separation and with a $d_{norm}$ value of zero.

The associated two-dimensional histograms being a combination of $d_i$ vs. $d_e$, referred to as "2D fingerprint plots", are a useful tool in identifying and comparing different kinds of intermolecular interactions in a given crystal structure [38]. The 2D fingerprint plots can be decomposed to highlight particular atom pair close contacts. This decomposition enables separation of contributions from different interaction types, which overlap in the full fingerprint. The 2D fingerprint plots, which analyze and quantify all the intermolecular contacts at the same time, revealed that the main intermolecular contacts around the title complex are Cl…H/H…Cl, H…H, C…H/H…C, C…C, Ni…Cl/Cl…Ni, O…H/H…O, N…H/H…N and Cl…C/C…Cl (Fig. 3).

The decomposed fingerprint plots into the separated intermolecular contacts show that the dominant contribution results from the Cl…H/H…Cl contacts, covering 30.4% of the of the total contacts around the global surface (features (1) in Fig. 3). This contribution suggests that these contacts are the driving forces in the crystal packing formation, and thus the shortest contact is represented by the two spikes at about ($d_i$ = 1.42 Å, $d_e$ = 0.82 Å and $d_i$= 0.82 Å, $d_e$ = 1.42 Å) with a distance of 2.24 Å, which could be attributed to the presence of the O1–H1o1…Cl2 intermolecular

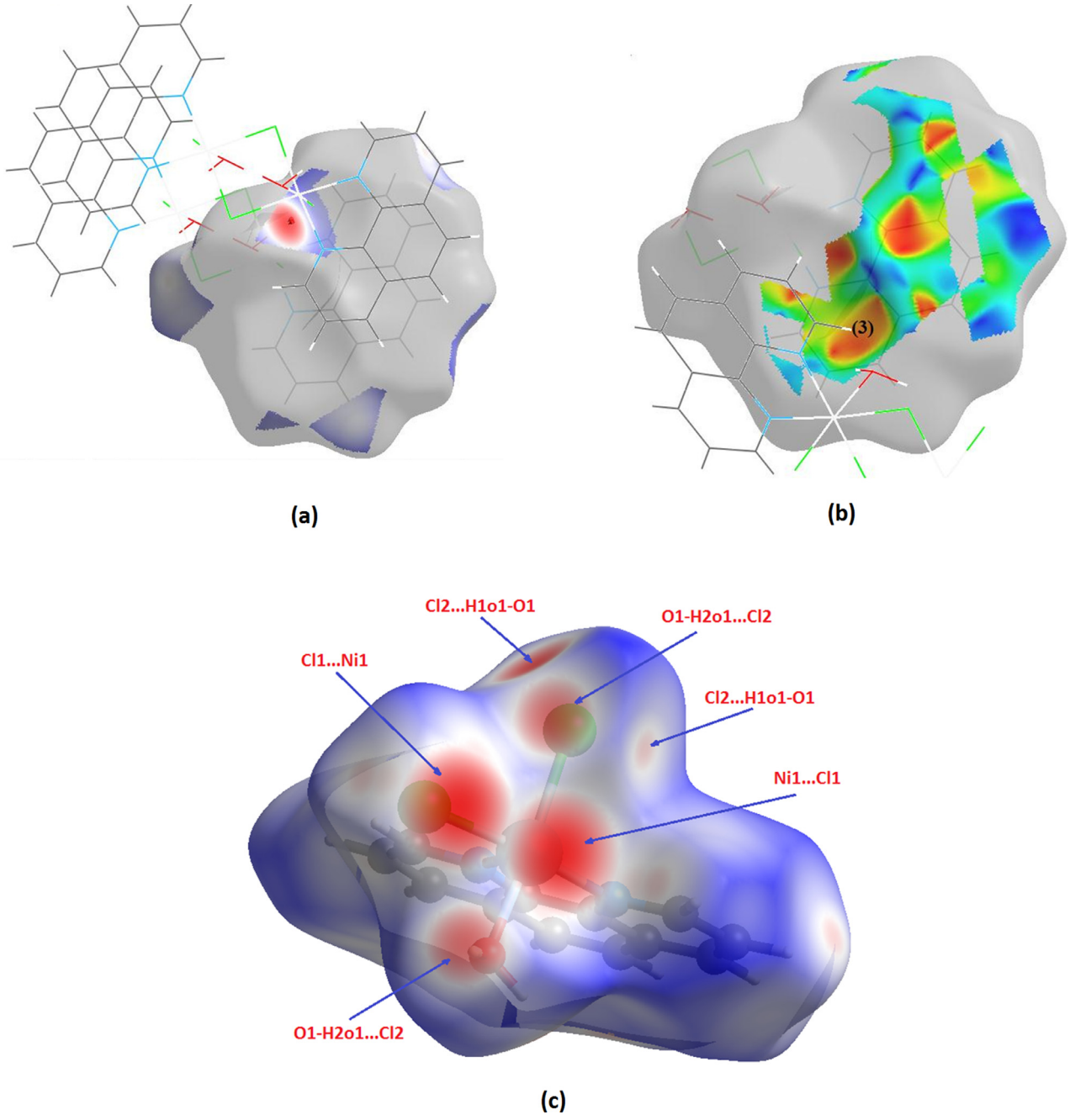


**Fig. 4.** (a) $d_{norm}$ representation mapped on the *Hirshfeld* surface and showing the shortest O…Cl/Cl…O contact; (b) *Shape index* representation visualizing the C3-H1c3…$\pi$ interactions; (c) Ni…Cl/Cl…Ni contacts visualized over the $d_{norm}$ function.

hydrogen bond (and its reciprocal interaction Cl2…H1o1–O1) discussed previously (Fig. 4a).

The H…H contacts, which are reflected in the middle of the scattered points (feature labeled (2) in Fig. 3 and covering the most area in the 2D fingerprint plots, have also the most significant contribution (together with the Cl…H/H…Cl contacts) to the total *Hirshfeld* surfaces; 30.1%. The shortest H…H contact appearing at ($d_i$ = 1.25 Å, $d_e$ = 1.20 Å) in the fingerprint plot, results from the C–H phenantroline hydrogens interacting with each other, namely the interaction C3–H1c3…H1c7–C7 (and its reciprocal interaction C7–H1c7…H1c3–C3 appearing at $d_i$ = 1.20 Å and $d_e$ = 1.25 Å). Furthermore, the C…H/H…C contacts represent the second most abundant type of interactions in the structure with 23%, and appear as two large wings in the 2D fingerprint plot (features labeled (3) in Fig. 3). The shortest contact of this type could be attributed to the C3–H1c3…$\pi$ interaction ($d_i + d_e \approx$ 2.7 Å) illustrated in Fig. 4b.

In addition, the C…C contacts, displayed as characteristic stacking kite (labeled (4) in Fig. 3), have less important weight in the crystal structure, which is underlined by its contribution of about 5.8%, and are mainly assigned to $\pi$…$\pi$ interactions. Therefore their shortest distance of about ($d_i + d_e \approx$ 3.2 Å) results from the $\pi$…$\pi$ interaction involving the C10 and C12 atoms. The decomposition of the fingerprint plot shows that both O…H/H…O and Ni…Cl/Cl…Ni contacts comprise only over 3% of the total *Hirshfeld* surface area (labels (5) and (6) in Fig. 3, respectively). The shortest O…H/H…O contact of ($d_i + d_e \approx$ 2.42 Å) is attributed to the reciprocal interaction O1…H1c1-C1/C1-H1c1…O1. Whereas, the Ni1…Cl1 interac-

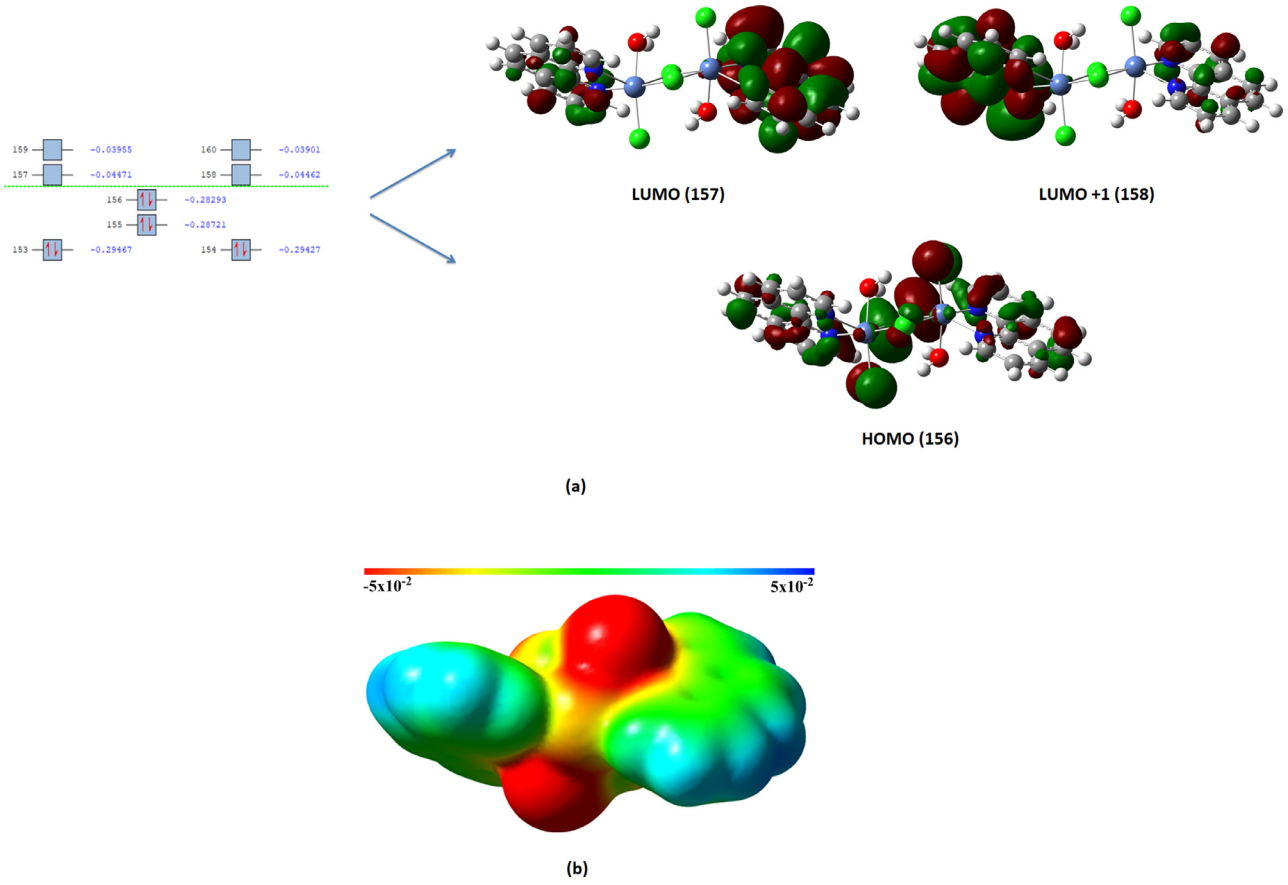


**Fig. 5.** (a) MOED and contour diagram of selected molecular orbitals calculated for the studied complex; (b) MEP map of the title complex.

tion (Fig. 4c) interprets the presence of the Ni…Cl/Cl…Ni contacts and is observed at about ($d_i + d_e \approx 2.44$ Å). The proportions of N…H/H…N and Cl…C/C…Cl contacts cover less than 3.0% of the total *Hirshfeld* surfaces and are highlighted by their shortest interactions; namely C1–H1c1…N1 ($d_i + d_e \approx 2.95$ Å) and C8…Cl2 ($d_i + d_e \approx 3.96$ Å), respectively. Whereas, the *Hirshfeld* surface of the title compound exhibit less than 1% of the non-conventional Ni…H/H…Ni, Cl…N/N…Cl and Cl…O/O…Cl contacts. Moreover, the O…Cl and N…Cl distances of the closest contacts range from 3.10 to 3.96 Å, which result from the interactions N2…Cl2 and O1…Cl2, respectively. The proportion of the different intermolecular contact types resulting from the *Hirshfeld* surface analysis of the title complex are shown in Fig. S1.

### *3.3. Structure optimization and contour plots of selected MOs and MEP map*

The title complex's structure was optimized by using one of the DFT function hybrids M06–2X method, with a mix basis set; LANL2DZ was used for $Ni^{2+}$ centers and 6–31G(d) for the other atoms in the complex. The structure at the ground state is shown in Fig. S2. Selected experimental and calculated bond lengths and bond angles of the environment of the $Ni^{2+}$ atoms are given in Table 3. Moreover, the full experimental and calculated geometric parameters are illustrated in Table S1.

According to the calculated results of Table 3, the bond lengths linking the metallic centers with their related atoms were calculated in the range 1.974–2.294 Å. Whereas, the optimized angles were found to vary from 77.7° to 173.0° around the Ni(II) atoms. The bond lengths show a maximum deviation of 0.1934 Å, observed for the Ni1–Cl2 bond length, which is not quite significant. Whereas, it is found that the maximum deviation value in the bond angles is 19.47°, which is associated to the Cl2–Ni1–N1 angle. This reveals a close agreement between the experimental structural parameters, the theoretical values and additionally with the values published earlier in the literature (Ni–Cl = 2.26 Å, Ni–*N* = 1.87–2.13 Å and Ni–*O* = 2.12–2.14 Å [39–43]). The slight deviation observed is attributed to the fact that the theoretical calculations have been carried out with an isolated molecule in the gaseous phase whereas the experimental values correspond to the molecule in the crystalline state.

The IR spectrum of the title complex was calculated and represented in Fig. S3. Additionally, the selected frequencies and their vibration modes are given in Table S2. The stretching frequency belonging to the O–H bond is obtained at 3610 and 3425 $cm^{-1}$. Additionally, the stretching of the (N–C) and (C–C) bonds are calculated at different frequencies, namely 1676, 1491 and 1126 $cm^{-1}$. As for the (Ni–O) stretching, it is calculated at 440 $cm^{-1}$.

The molecular orbital energy diagram (MOED) is very important in the determination of the electronic properties. The diagram shows that HOMO, LUMO and LUMO+1 are important molecular orbitals (MOs) for the studied complex. The MOED and the contour plots of significant MOs are represented in Fig. 5.

The HOMO electrons are mainly delocalized on the chlorine atoms as shown in Fig. 5a; they are thus active for any interaction. As for the unoccupied molecular orbitals, if the investigated compound accepts electrons they will be delocalized on the rings. The contour plots of selected molecular orbitals are important to determine the active sites of the studied complex. According to Fig. 5a, the chlorine atoms are appropriate for nucleophilic attacks. On the other hand, the $\pi$ electrons are active for any interactions. Another significant illustration is the molecular electrostatic po-

**Table 3**
Selected experimental and calculated geometric parameters within the title complex.

| Bond Lengths (Å) | | | | | |
|---|---|---|---|---|---|
| | Experimental | Calculated | | Experimental | Calculated |
| Ni1–Cl1 | 2.3983(6)/2.4116(6) | 2.294 | Ni1–N1 | 2.0636(19) | 2.077 |
| Ni1–Cl2 | 2.4394(6) | 2.246 | Ni1–N2 | 2.0648 (17) | 1.974 |
| Ni1–O1 | 2.125(1) | 1.992 | – | – | – |
| Bond Angles (°) | | | | | |
| Cl1–Ni1–Cl1$^{i}$ | 89.932(19) | 101.7 | Cl2–Ni1–N2 | 92.56(5) | 91.2 |
| Cl1–Ni1–Cl2 | 91.426(19) | 92.9 | Cl2–Ni1–N1 | 92.73(5) | 112.2 |
| Cl1–Ni1–O1 | 87.45(5) | 90.0 | O1–Ni1–N2 | 91.70(7) | 87.6 |
| Cl1–Ni1–N2 | 174.30(5) | 173.0 | O1–Ni1–N1 | 87.58(6) | 83.1 |
| Cl1–Ni1–N1 | 95.21(5) | 95.5 | N1–Ni1–N2 | 80.52(7) | 77.7 |
| Cl2–Ni1–O1 | 175.73(5) | 163.0 | – | – | – |

*Symmetry code: (i): x, y − 1, z.*

tential (MEP) map (Fig. 5b) which playacts an important role in the determination of the active sites on the molecular surface. Especially, the electronic charge distribution can be easily seen by the MEP map because the electrostatic potential (ESP) charges are calculated to obtain the MEP map. According to Fig. 5b, there are more electrons around the chlorine atoms compared to the rest of the molecule. Additionally, the $\pi$ electrons delocalization demonstrates the activity of the studied complex, which is in agreement with the results already showed in Fig. 5a.

## 4. Conclusions

In this work, a binuclear nickel complex, $NiCl_2(H_2O)(C_{12}N_2H_8)$, was synthesized in solution. Its crystal structure was described in terms of $Ni_2Cl_4(H_2O)_2(Phen)_2$ dimmers interacting through weak intermolecular O–H…Cl hydrogen bonds. The *Hirshfeld* surface analysis of the various intermolecular contacts in the framework of the title compound was discussed, showing a rich variety of contacts namely: Cl…H/H…Cl, H…H, C…H/H…C, C…C, Ni…Cl/Cl…Ni, O…H/H…O, N…H/H…N and Cl…C/C…Cl reciprocal interactions. Quantum chemical investigations were performed and the structural properties were examined in detail. Additionally, the active sites were determined by the calculation of contour plots of the molecular orbitals and the MEP map.

## Declaration of Competing Interest

The authors declare that they have no known competing financial interests or personal relationships that could have appeared to influence the work reported in this paper.

## CRediT authorship contribution statement

**Brahim El Bali:** Conceptualization, Writing - original draft, Writing - review & editing. **Mohammed Lachkar:** Formal analysis, Validation. **Amani Direm:** Writing - original draft, Writing - review & editing, Visualization. **Esra Çetiner:** Visualization. **Koray Sayin:** Resources, Writing - original draft, Funding acquisition. **Michal Dusek:** Investigation, Validation.

## Acknowledgments

The crystallographic part was supported by the project 18-10438S of the Czech Science Foundation using instruments of the ASTRA laboratory established within the Operation program Prague Competitiveness - project CZ.2.16/3.1.00/24510.

## Supplementary materials

Supplementary material associated with this article can be found, in the online version, at doi:10.1016/j.molstruc.2020.129576.

## References

[1] G. Wilkinson, R.D. Gillard, J.A. McCleverty, Comprehensive Coordination Chemistry, Eds., 6, Pergamon Press, Oxford, UK, 1987.
[2] C. Bazzicalupi, A. Bencini, V. Fusi, C. Giorgi, P. Paoletti, B. Valtancoli, Lead complexation by novel phenanthroline-containing macrocycles, J. Chem. Soc., Dalton Trans. (1999) 393–400.
[3] P.G. Sammes, G. Yahioglu, 1, 10-Phenanthroline: a versatile ligand, Chem. Soc. Rev. 23 (1994) 327–334.
[4] C.E.A. Palmer, D.R. McMillin, C. Kirmaier, D. Holten, Flash photolysis and quenching studies of copper(I) systems in the presence of Lewis bases: inorganic examples, Inorg. Chem. 26 (19) (1987) 3167–3170.
[5] S. Sakaki, G. Koga, K. Ohkubo, Successful photocatalytic reduction of methylviologen ($MV^{2+}$) with $[Cu(NN)(PPh_3)_2]^+$ (NN= 2,9-dimethyl-1,10-phenanthroline or 4,4′,6,6′-tetramethyl-2,2′-bipyridine) upon near-UV-light irradiation and a novel solvent effect on its catalytic activity, Inorg. Chem. 25 (14) (1986) 2330–2333.
[6] D.M. Walba, Q.Y. Zheng, K. Shilling, Experimental studies on the hook and ladder approach to molecular knots: synthesis of a topologically chiral cyclized hook and ladder, J. Am. chem. soc. 114 (1992) 6259–6260.
[7] S.S. Zhu, T.M. Swager, Conducting polymetallorotaxanes: metal ion mediated enhancements in conductivity and charge localization, J. Am. Chem. Soc. 119 (51) (1997) 12568–12577.
[8] D.J. Cardenas, P. Gavena, J.P. Sauvage, Construction of interlocking and threated rings using 2 different transition-metals as templating and connecting centers-catenanes and roxananes incoporating ru(terpy)(2)-units in their framework, J. Am. Chem. Soc. 119 (11) (1997) 2656–2664.
[9] R. Ziessel, A. Harriman, J. Suffert, M.T. Youinou, A.D. Cian, J. Fischer, Kupfer(I)-Helicate mit verbrückenden statt chelatisierenden Oligopyridinliganden, Angewandte Chemie 109 (22) (1997) 2621–2623.
[10] C.O.D. Buchecker, J.P. Sauvage, A synthetic molecular trefoil knot, Angewandte Chemie 28 (2) (1989) 189–192.
[11] F. Sallas, A. Marsura, V. Petot, I. Pintér, J. Kovács, L. Jicsinszky, Synthesis and study of new $\beta$-cyclodextrin 'dimers' having a metal coordination center and carboxamide or urea linkers, Helv. Chim. Acta 81 (3–4) (1998) 632–645.
[12] L.G. Bachas, L. Cullen, R.S. Hutchins, D.L. Scott, Synthesis, characterization and electrochemical polymerization of eight transition-metal complexes of 5-amino-1,10-phenanthroline, J. Chem. Soc., Dalton Trans. (1997) 1571–1578.
[13] J. Tammiku, P. Burk, A. Tuulmets, 1,10-Phenanthroline and its complexes with magnesium compounds. Disproportionation equilibria, J. Phys. Chem. A 105 (37) (2001) 8554–8561.
[14] P. Heffeter, M.A. Jakupec, W. Körner, S. Wild, N.G. von Keyserlingk, L. Elbling, H. Zorbas, A. Korynevska, S. Knasmüller, H. Sutterlüty, M. Micksche, B.K. Keppler, W. Berger, Anticancer activity of the lanthanum compound [tris(1,10-phenanthroline) lanthanum(III)]trithiocyanate (KP772; FFC24), Biochem. Pharmacol. 71 (4) (2006) 426–440.
[15] K. Kobayashi, H. Ohtsu, K. Nozaki, S. Kitagawa, K. Tanaka, Photochemical properties and reactivity of a Ru compound containing an NAD/NADH-functionalized 1,10-phenanthroline ligand, Inorg. Chem. 55 (5) (2016) 2076–2084.
[16] A. Bencini, V. Lippolis, 1, 10-Phenanthroline: a versatile building block for the construction of ligands for various purposes, Coord. Chem. Rev. 254 (17) (2010) 2096–2180.
[17] A. Abebe, M. Atlabachew, M. Liyew, E. Ferede, Synthesis of organic salts from 1,10-phenanthroline for biological applications, Cogent Chem. 4 (1) (2018) 1476077, doi:10.1080/23312009.2018.1476077.
[18] P. Alrejaa, N. Kaur, Recent advances in 1,10-phenanthroline ligands for chemosensing of cations and anions, RSC Adv. 6 (2016) 23169–23217.

[19] D.B. Eni, D.M. Yufanyi, J.H. Nono, C.D. Tabong, M.O. Agwara, Synthesis, characterization and thermal properties of 1,10-phenanthroline mixed-ligand complexes of cobalt(II) and copper(II): metal-mediated transformations of the dicyanamide ion, Chem. Pap. 74 (2020) 3003–3016.
[20] AgilentCrysAlis PRO, Agilent Technologies, Yarnton, England, 2010.
[21] A. Altomare, M.C. Burla, M. Camalli, G.L. Cascarano, C. Giacovazzo, A. Guagliardi, A.G.G. Moliterni, G. Polidori, R. Spagna, SIR97 : a new tool for crystal structure determination and refinement, J. Appl. Cryst. 32 (1999) 115–119.
[22] V. Petříček, M. Dušek, L. Palatinus, Crystallographic computing system JANA2006: general features, Z. Kristallogr. 229 (5) (2014) 345–352.
[23] K. Brandenburg, H. Putz, DIAMOND Version 3, Crystal Impact GbR, Bonn, Germany, 2005.
[24] M.A. Spackman, D. Jayatilaka, Hirshfeld surface analysis, Cryst. Eng. Comm. 11 (2009) 19–32.
[25] S.K. Wolff, D.J. Grimwood, J.J. McKinnon, M.J. Turner, D. Jayatilaka, M.A. Spackman, CrystalExplorer, 3, University of Western, Australia: Perth, Australia, 2014.
[26] R.D. Dennington II, T.A. Keith, J.M. Millam, GaussView 6.0, Wallingford, CT, 2016.
[27] M.J. Frisch, G.W. Trucks, H.B. Schlegel, G.E. Scuseria, M.A. Robb, J.R. Cheeseman, G. Scalmani, V. Barone, B. Mennucci, G.A. Petersson, H. Nakatsuji, M. Caricato, X. Li, H.P. Hratchian, A.F. Izmaylov, J. Bloino, G. Zheng, J.L. Sonnenberg, M. Hada, M. Ehara, K. Toyota, R. Fukuda, J. Hasegawa, M. Ishida, T. Nakajima, Y. Honda, O. Kitao, H. Nakai, T. Vreven, J.A. Montgomery Jr., J.E. Peralta, F. Ogliaro, M. Bearpark, J.J. Heyd, E. Brothers, K.N. Kudin, V.N. Staroverov, R. Kobayashi, J. Normand, K. Raghavachari, A. Rendell, J.C. Burant, S.S. Iyengar, J. Tomasi, M. Cossi, N. Rega, J.M. Millam, M. Klene, J.E. Knox, J.B. Cross, V. Bakken, C. Adamo, J. Jaramillo, R. Gomperts, R.E. Stratmann, O. Yazyev, A.J. Austin, R. Cammi, C. Pomelli, J.W. Ochterski, R.L. Martin, K. Morokuma, V.G. Zakrzewski, G.A. Voth, P. Salvador, J.J. Dannenberg, S. Dapprich, A.D. Daniels, Ö. Farkas, J.B. Foresman, J.V. Ortiz, J. Cioslowski, D.J. Fox, Gaussian 09, Gaussian AS64L-G09RevD.01, Gaussian, Inc., Wallingford CT, 2010.
[28] M.J. Frisch, G.W. Trucks, H.B. Schlegel, G.E. Scuseria, M.A. Robb, J.R. Cheeseman, G. Scalmani, V. Barone, G.A. Petersson, H. Nakatsuji, X. Li, M. Caricato, A.V. Marenich, J. Bloino, B.G. Janesko, R. Gomperts, B. Mennucci, H.P. Hratchian, J.V. Ortiz, A.F. Izmaylov, J.L. Sonnenberg, D. Williams-Young, F. Ding, F. Lipparini, F. Egidi, J. Goings, B. Peng, A. Petrone, T. Henderson, D. Ranasinghe, V.G. Zakrzewski, J. Gao, N. Rega, G. Zheng, W. Liang, M. Hada, M. Ehara, K. Toyota, R. Fukuda, J. Hasegawa, M. Ishida, T. Nakajima, Y. Honda, O. Kitao, H. Nakai, T. Vreven, K. Throssell, J.A. Montgomery Jr., J.E. Peralta, F. Ogliaro, M.J. Bearpark, J.J. Heyd, E.N. Brothers, K.N. Kudin, V.N. Staroverov, T.A. Keith, R. Kobayashi, J. Normand, K. Raghavachari, A.P. Rendell, J.C. Burant, S.S. Iyengar, J. Tomasi, M. Cossi, J.M. Millam, M. Klene, C. Adamo, R. Cammi, J.W. Ochterski, R.L. Martin, K. Morokuma, O. Farkas, J.B. Foresman, D.J. Fox, Gaussian 16, Revision B.01, Gaussian, Inc., Wallingford CT, 2016.
[29] M.H. Jamroz, Vibrational energy distribution analysis VEDA 4, Warsaw, 2004–2010.
[30] A. Ferrari, A. Braibanti, G. Bigliardi, Refinement of the crystal structure of Ni Cl2 and of unit-cell parameters of some anhydrous chlorides of divalent metals, Acta Cryst. 16 (1963) 846–847.
[31] B. Morosin, An X-ray diffraction study on nickel(II) chloride dehydrate, Acta Cryst. 23 (1967) 630–634.
[32] E.V. Stroganov, I.I. Kozhina, S.N. Andreev, A.B. Koljadin, Crystal structure of hydrated salts of transition metals. II Structure of $NiCl_2.4H_2O$., Vestnik Leningradskogo Universiteta, Fizika, Khimiya 15 (1960) 130–137.
[33] R. Kleinberg, Crystal structure of $NiCl_2(H_2O)_6$ at room temperature and 4.2K by neutron diffraction, J. Chem. Phys. 50 (1969) 4690–4696.
[34] W.P. Davey, RbBr, NiO, CsCl, T1C1, Phys. Rev. 17 (1921) 402–403.
[35] J. Bernstein, R.E. Davis, L. Shimoni, N.-L. Chang, Patterns in hydrogen bonding functionality and graph set analysis in crystals, Angew. Chem. Int. Ed. Engl. 34 (1995) 1555–1573.
[36] J.J. McKinnon, M.A. Spackman, A.S. Mitchell, Novel tools for visualizing and exploring intermolecular interactions in molecular crystals, Acta Crystallogr. B60 (2004) 627–668.
[37] J.J. McKinnon, D. Jayatilaka, M.A. Spackman, Towards quantitative analysis of intermolecular interactions with Hirshfeld surfaces, Chem. Commun. (2007) 3814–3816.
[38] M.A. Spackmann, J.J. McKinnon, Fingerprinting intermolecular interactions in molecular crystals, Cryst. Eng. Comm. 4 (2002) 378–392.
[39] A.R. Cabrera, I. Martinez, C.G. Daniliuc, G.B. Galland, C.O. Salas, R.S. Rojas, New air stable cationic methallyl Ni complexes bearing imidoyl-indazole carboxylate ligand: synthesis, characterization and their reactivity towards ethylene, J. Mol. Catal. A 414 (2016) 19–26.
[40] S. Ando, N. Nakano, H. Matsunaga, T. Ishizuka, Synthesis and catalytic activities of Ni complexes bearing a novel N–C–N pincer ligand containing NHC with a bicyclic motif, J. Organomet. Chem. 913 (2020) 121200.
[41] T. Hamaguchi, I. Ando, Synthesis and characterisation of a new six-coordinated thermochromic Ni complex, Inorganica Chim Acta 427 (2015) 144–149.
[42] N.K. Senaratne, T.M. Mwania, C.E. Moore, D.M. Eichhorn, Ni complexes of N2S ligands with amine/imine and amine/amide donors with relevance to the active site of Ni superoxide dismutase, Inorganica Chim Acta 476 (2018) 27–37.
[43] A. Mrutu, K.I. Goldberg, R.A. Kemp, Synthesis and characterization of a dinuclear Ni complex containing a bridging CNC pincer ligand, Inorganica Chim Acta 364 (1) (2010) 115–119.

# Electronic Supplementary Information

of the manuscript entitled :

# Experimental and computational studies of Di-μ-chlorido-bis-[chlorido(1,10-phenanthroline-κ2*N*,*N*′)nickel(II)] $NiCl_2(H_2O)(C_{12}N_2H_8)$: Crystal structure, quantitative analysis of the intermolecular interactions and electronic properties

**Brahim EL BALI [1], Mohammed LACHKAR [2], Amani DIREM [3*], Esra ÇETİNER [4], Koray SAYIN [4] & Michal DUSEK [5]**

[1] Independent scientist, ORCID : 0000-0001-6926-6286 ; Email : b_elbali@yahoo.com

[2] Laboratoire d'Ingénierie des Matériaux Organométalliques et Moléculaires, Unité Associée au CNRST (URAC 19), Faculté des Sciences, Université Sidi Mohamed Ben Abdellah, B.P.1796 (Atlas), 30000 Fès, Morocco.

[3] Laboratory of Structure, Properties and Intermolecular Interactions LASPI$^2$A, Department of Matter Sciences, Faculty of Sciences and Technology, Abbes Laghrour University Khenchela, 40.000 Algeria.

[4] Department of Chemistry, Faculty of Science, Cumhuriyet University 58140 Sivas – Turkey.

[5] Institute of Physics of the Czech Academy of Sciences, Na Slovance 2, 182 21 Praha 8, Czech Republic.

* Corresponding Author : Amani Direm (ORCID : 0000-0002-6347-9173)
E-mail : amani_direm@yahoo.fr
Tel. : +213.772.33.02.87

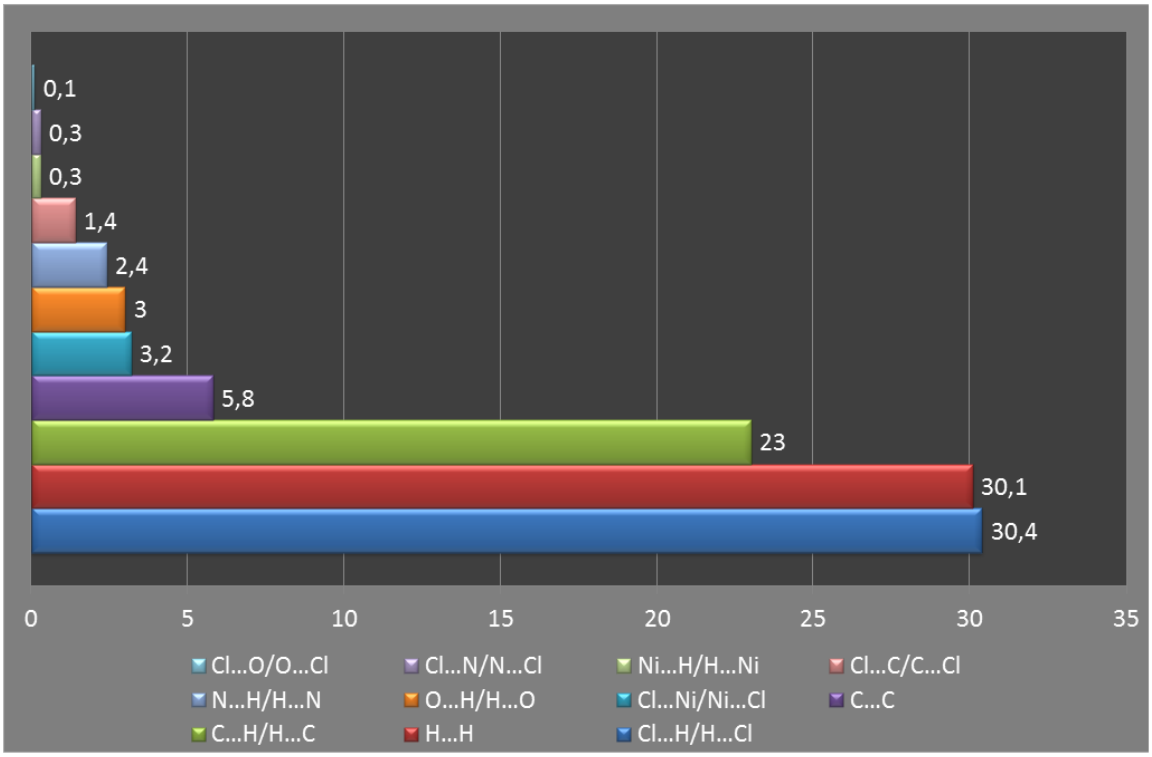


**Fig. S1. Schematic illustration of the decomposed fingerprint plots of the title compound.**

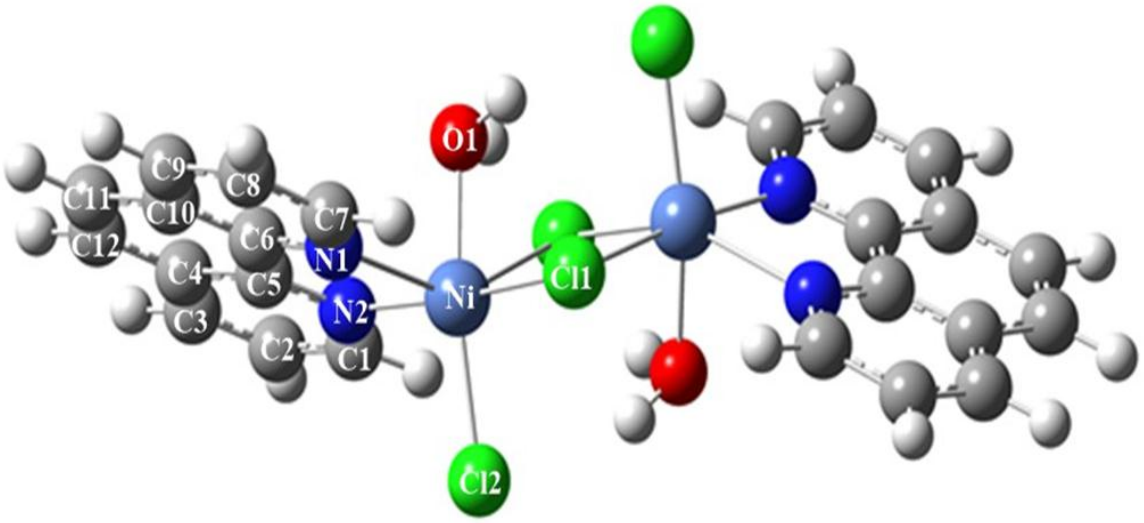


**Fig. S2. Optimized structure of the title complex in vacuum at mentioned calculation levels.**

**Table S1.** Full experimental and calculated geometric parameters of the title complex.

| **Bond Lengths (Å)** | | | | | |
|---|---|---|---|---|---|
| | Experimental | Calculated | | Experimental | Calculated |
| Ni1─Cl1 | 2.3983(6)/2.4116(6) | 2.294 | Ni1─N1 | 2.0636(19) | 2.077 |
| Ni1─Cl2 | 2.4394(6) | 2.246 | Ni1─N2 | 2.0648 (17) | 1.974 |
| Ni1─O1 | 2.125(1) | 1.992 | C3─C1 | 1.401(3) | 1.409 |
| C3─N1 | 1.324(3) | 1.316 | C5─C9 | 1.439(3) | 1.449 |
| C1─C2 | 1.368(3) | 1.375 | C5─C4 | 1.406(3) | 1.410 |
| C2─C4 | 1.411(3) | 1.411 | C5─N1 | 1.359(3) | 1.348 |
| C9─C10 | 1.405(3) | 1.408 | C4─C11 | 1.439(3) | 1.437 |
| C8─C6 | 1.401(3) | 1.405 | C10─C12 | 1.436(3) | 1.436 |
| C6─C7 | 1.368(3) | 1.374 | C11─C12 | 1.352(3) | 1.355 |
| C7─C10 | 1.406(3) | 1.410 | - | - | - |
| **Bond Angles (°)** | | | | | |
| Cl1─Ni1─Cl1$^{i}$ | 89.932(19) | 101.7 | Cl2─Ni1─N2 | 92.56(5) | 91.2 |
| Cl1─Ni1─Cl2 | 91.426(19) | 92.9 | Cl2─Ni1─N1 | 92.73(5) | 112.2 |
| Cl1─Ni1─O1 | 87.45(5) | 90.0 | O1─Ni1─N2 | 91.70(7) | 87.6 |
| Cl1─Ni1─N2 | 174.30(5) | 173.0 | O1─Ni1─N1 | 87.58(6) | 83.1 |
| Cl1─Ni1─N1 | 95.21(5) | 95.5 | N1─Ni1─N2 | 80.52(7) | 77.7 |
| Cl2─Ni1─O1 | 175.73(5) | 163.0 | Ni1─N2─C9 | 112.82(13) | 118.1 |
| Ni1─N2─C8 | 129.03(15) | 121.6 | Ni1─N1─C5 | 112.80(13) | 106.2 |
| Ni1─N1─C3 | 128.78(15) | 134.9 | C1─C2─C4 | 119.5(2) | 119.7 |
| C1─C3─N1 | 122.6(2) | 121.9 | C5─C4─C11 | 118.6(2) | 119.8 |
| C3─C1─C2 | 119.5(2) | 119.0 | C4─C5─C9 | 120.13(18) | 119.3 |
| C2─C4─C11 | 124.2(2) | 122.5 | C10─C9─N2 | 123.17(19) | 122.7 |
| C5─C9─C10 | 119.87(19) | 119.3 | N2─C8─C6 | 122.8(2) | 122.8 |
| C8─C6─C7 | 119.1(2) | 118.6 | C4─C5─N1 | 122.94(19) | 121.3 |
| C6─C7─C10 | 119.9(2) | 119.2 | C9─C10─C7 | 116.9(2) | 117.2 |
| C7─C10─C12 | 124.2(2) | 122.1 | C10─C12─C11 | 121.3(2) | 120.7 |
| C4─C11─C12 | 121.2(2) | 121.0 | C3─N1─C5 | 118.40(19) | 120.2 |

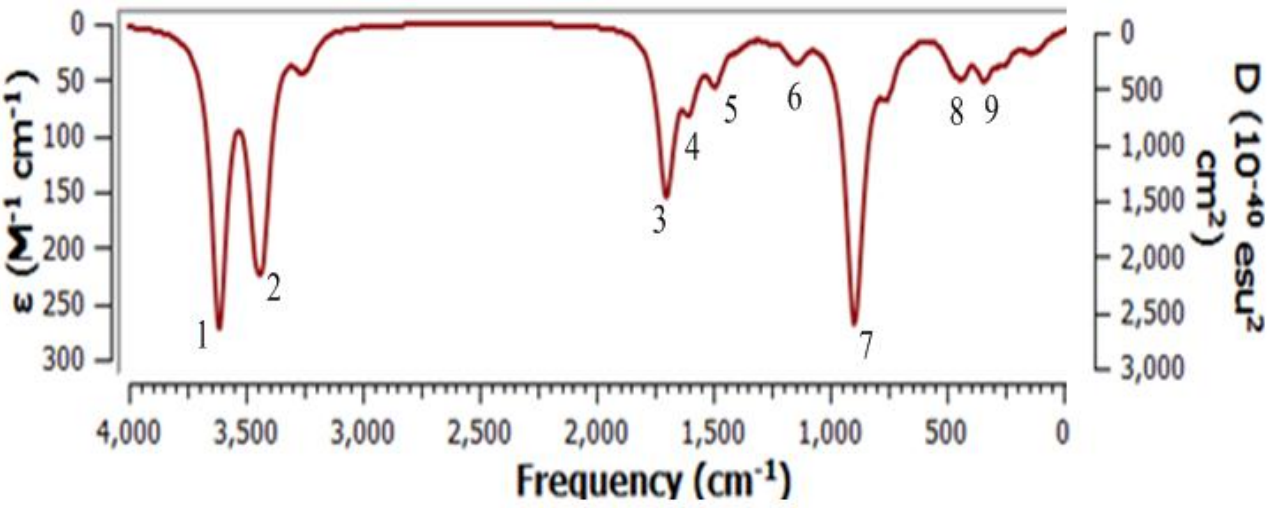


**Fig. S3. Calculated IR spectrum of the title complex.**

**Table S2.** Frequencies and vibration modes of the selected bands in the IR spectrum.

| **Bands** | **Frequencies ($cm^{-1}$)** | **Vibration Modes** |
|---|---|---|
| 1 | 3610 | Stretching (O─H) |
| 2 | 3425 | Stretching (O─H) |
| 3 | 1703 | Bending (H─O─H) |
| 4 | 1676 | Stretching (N─C); Stretching (C─C) |
| 5 | 1491 | Stretching (N─C); Bending (H─C─C) |
| 6 | 1126 | Stretching (C─C) |
| 7 | 440 | Stretching (Ni─O) |
| 8 | 345 | Stretching (Ni─Cl) |
| 9 | 211 | Stretching (Ni─N) |